

# Effect of cracking due to thermal treatment in cement-based materials on chloride diffusion and gas permeability processes

S. Caré

Laboratoire Central des Ponts et Chaussées, Paris, France

**ABSTRACT:** In this paper, the real microstructure of the concrete is taken into account, particularly cracking obtained by thermal treatment. Our experimental studies aim at determining the influence of cracking state on transport by chloride diffusion and gas permeability processes and at linking these transport properties to microstructure (cracking and porosity). The studied materials are two cement pastes (W/C=0.35 and 0.45). The chloride diffusion and gas permeability tests are performed on cracked and uncracked materials. The thermal treatment allows us to induce localized microcracking characterized by width of hundred micrometers. Our results show that the transport properties are modified by thermal treatment. But these modifications may be explained by the modification of the porosity and the cracking has little influence on the transport properties.

## 1 INTRODUCTION

The durability of concrete structures is a very important issue in actual concrete research. Many predictive models are developed and experimental works are carried out to predict service life of concrete structures. Concrete structures are exposed to service load (mechanical actions) and to chemical and physical actions (thermal or moisture gradients) due to their exposure to environment. These actions lead to diffuse microcracking characterized by width of ten micrometers or so and by localized microcracking (which forms a network) characterized by width of hundred micrometers. According to Gérard & Marchand (2000), it has been shown that the continuity of the crack network and the mean aperture of cracks have a marked influence on the material permeability (for cracking induced by mechanical loading). Nevertheless, few works consider the ability of concrete to be deteriorated by cracking and deal with the incidence of cracks on diffusion properties. Furthermore, the few reports published on the subject are more and less contradictory.

The aim of this study is to determine the influence of the cracking state on transport properties. The studied materials are two cement pastes with different Water/ Cement (W/C) ratio. Localized cracks are induced by thermal treatment and form an isotropic network characterized by the mean aperture (or width) of the cracks and the mean crack spacing. In our work, different experiments are carried out. On one hand, gas permeability and chloride penetration

tests are performed. And on the other hand, microstructure of studied materials is analyzed by mercury intrusion porosimetry (MIP) and by optical microscopy.

## 2 TEST PROGRAM

### 2.1 Materials

The tested materials are two cement pastes (with different water/cement ratio) cast with a Portland cement, European grade CEM I. The water/cement ratio of the cement paste labeled CO is 0.35 and the one of the cement paste labeled CN is 0.45.

Specimens are molded in 70 x 100 mm PVC cylinders. Moulds are then rotated for 24 h to avoid any segregation of the mixtures. After demoulding, the samples are wrapped in two superimposed adhesive aluminium sheets in order to ensure a suitable watertightness until the beginning of experiments. The materials are more than 6 month old at the beginning of the experiments so that the microstructure can be considered fixed during diffusion and permeability tests.

The cement pastes are perfectly dried at different temperatures (45°C, 80°C and 105°C) to generate cracking. The perfectly dry condition may be defined as constant mass (of samples), i.e. less than 0.5% variation of mass during 24 hours at each temperature. After drying, the materials are exposed in water during 24 h 00 so that materials may be considered as saturated before diffusion and permeability tests

and microstructural characterization. Four types of samples are then examined: the sample 1A for the initial state, the 1B for the material dried at 45°C, the 2A for the one at 80°C and the 2B for the one at 105°C. Chloride penetration tests are performed on specimens of size 25 mm x 50 mm x 50 mm. For the gas permeability tests, only the 1A and 2B samples are tested and the tested samples are 70 mm x 20 mm cylinders.

## 2.2 Experimental procedures

### 2.2.1 Microstructure

Porosity of the studied materials is investigated by Mercury Intrusion Porosimetry (MIP) measurements. Before the testing, the samples are submerged directly into liquid nitrogen for 15 minutes and then are vacuum dried at -55°C - for 24 h 00.

Mercury Intrusion Porosimetry (MIP) measurements are carried out using a CE Instruments apparatus. The instrument is capable of a minimum intruding pressure of 2.6 kPa and a maximum of 200 MPa, so that the pore radius ranges from 3.7 nm to 60 µm. The contact angle of 141.3° is used in the computations.

Cracking is observed by a technique using dye impregnation according to Hornain (1996). The procedure involves the impregnation of a section with a colored dye diluted in an alcohol. After a short impregnation period, the section is polished under water. Cracks are then observed using optical microscopy.

### 2.2.2 Permeability

Gas permeability tests are performed with variable head permeameter (Figure 1) developed by LCPC (Caré 2000) according to Yssorche (1995). The permeability  $K$  ( $m^2$ ) is measured from Darcy's law (Eq.1):

$$Q = \frac{-KA}{\mu} \frac{dP}{dz} \quad (1)$$

where  $Q$  = volume flow rate of air ( $m^3.s^{-1}$ );  $A$  = cross-sectional area of the specimen ( $m^2$ );  $\mu$  = viscosity ( $N.s.m^{-2}$ ) of the fluid at test temperature; and  $dP/dz$  = pressure gradient ( $N.m^{-3}$ ).

Theoretical considerations lead to the determination of the permeability  $K$  (Yssorche 1995), thus:

$$K = \frac{\mu s L}{\rho_w A g t} \ln\left(\frac{h(0)}{h(t)}\right) \quad (2)$$

where  $s$  = cross-sectional area of the tube ( $m^2$ );  $L$  = thickness of the specimen (m) in the direction of flow;  $\rho_w$  = relative density of water ( $kg.m^{-3}$ );  $t$  = time of measure (s);  $h(0)$  = height (m) of water in the tube at the pressure  $P(0)$  at time  $t=0$ ; and  $h(t)$  = height (m)

of water in the tube at the pressure  $P(t)$  at time  $t$ .

A depressure is generated between the top of the specimen (at the pressure  $P_A$  equal to the atmospheric pressure) and the bottom of the specimen thanks a vacuum pump. At time  $t=0$  ( $P(0) \approx 0.1$  bar), the vacuum pump is stopped so that air can cross the specimen at the volume flow rate  $Q$ . The permeability  $K$  is obtained by the measure of the time  $t$  necessary to reach the pressure  $P(t)$  or the height  $h(t)$ .

Before the permeability tests can be carried out, the specimens have to be desaturated, so the prepared specimens are brought to the same moisture condition. Specimens are put into sealed desiccators where the relative humidity (RH) is controlled by saturated salt solution. The samples are dried at  $T=20$  °C, at about RH 90.4% for a period of about 100 days.

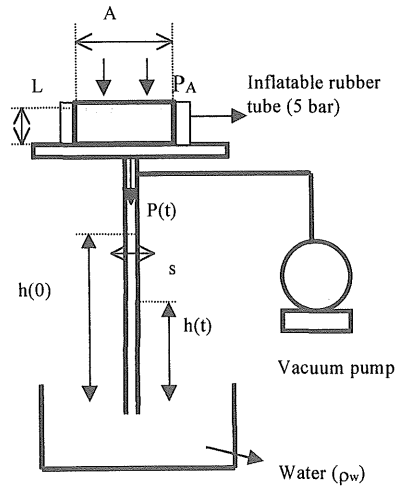


Figure 1: Experimental set up for gas permeability test.

### 2.2.3 Chloride diffusion

For the characterization of the chloride ingress, diffusion tests (non steady-state regime) are carried out on each mixture protected from moisture exchange, except for the bottom surface, intended to be in contact with a chloride solution (Figure 2). The NaCl solution (30 g/L) is changed every week. For this experimental set up, the capillary suction is considered as negligible.

After 3 weeks of diffusion, the chloride penetration is examined according to a colorimetric method (Maultzsch's procedure in Henry (2000)). The cement paste specimen is split by dry sawing and then a revealer (potassium dichromate) and a reactive (silver nitrate) are sprayed in the face perpendicular to the chloride-exposed surface. The chloride penetra-

tion front is determined by the color change, which detects the chloride ions. This method allows us to determine the depth of penetration of chloride ions  $X_{cl}$ . The penetration depth  $X_{cl}$  corresponds to the distance between the chloride-exposed surface and the border line between the two zones (zone without chloride ions and zone with chloride ions). On the assumption that the (soluble) chloride concentration at the color change border is the same for all specimens, this method appears to be a quick tool to compare chloride penetration in cracked and uncracked materials.

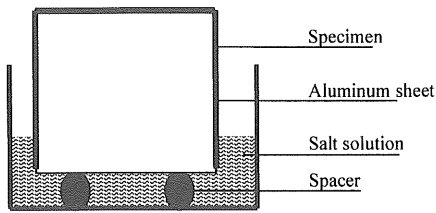


Figure 2: Experimental set up for diffusion test.

### 3 RESULTS AND DISCUSSION

#### 3.1 Microstructure

Microstructure of studied materials is analyzed by mercury intrusion porosimetry (MIP) and by optical microscopy.

##### 3.1.1 Porosity

The pore structure of all specimens is characterized by mercury intrusion porosimetry (MIP) and is given in Figure 3 and in Table 1.

Table 1. Porosity measurements.  $\Phi$  is the total porosity (%) and  $d_c$  is the critical diameter (nm) measured by MIP.

	CO		CN	
	$\Phi$ (%)	$d_c$ (nm)	$\Phi$ (%)	$d_c$ (nm)
1A	9.8	40	10.6	20
1B	10.0	40	15.9	30
2A	12.7	120	17.7	80
2B	18	120	21.8	80

For each specimen, one sample is tested. The Figure 3 presents the pore size distribution of the cement pastes labeled CN-1A, -2B (Figure 3a) and CO-1A, -2B (Figure 3b). The Table 1 gives the porosity  $\Phi$  (%) and the critical diameter  $d_c$  (nm) for each specimen. The diameter  $d_c$  is the critical diameter defined as the diameter, which corresponds to the maximum of porosity given by the pore size distribution.

The thermal treatment tends to modify the pore structure: on one hand the overall distributions are

shifted towards the coarser pores, i.e.  $d_c$  increases with the temperature of the thermal treatment and on the other hand the total porosity  $\Phi$  increases with the temperature of the thermal treatment.

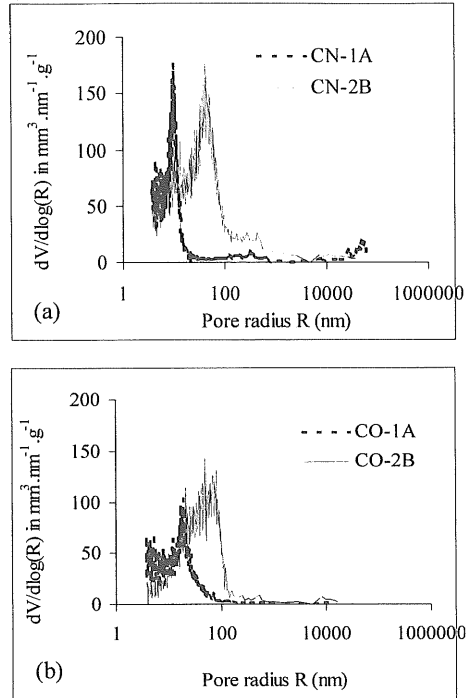


Figure 3: Pore size distribution measured by MIP on the specimens CN-1A, -2B (Figure 3a) and CO-1A, -2B (Figure 3b) with  $d_c=2R$ .

##### 3.1.2 Crack network

The cracking network is characterized according to a technique using red dye impregnation. An example for the specimen CO-2B is given in Figure 4.

Observations show that there are no cracks for the specimens CO-1A and CN-1A compared to the others specimens. The cracking network is seen to be about the same for all specimens (1B, 2A, 2B). The cracks are interconnected and form an isotropic network of a more and less polygonal shape, which is characterized by their mean aperture (or width)  $L_w$  and the mean crack spacing  $L_m$  (Figure 4). The mean crack spacing  $L_m$  is about 10-15 mm. The crack width  $L_w$  measured by optical microscope ranges from 50 to 100  $\mu\text{m}$  and is about the same for most of the major cracks. Although cracks appear to be continuous at low magnification, discontinuities are observed at high magnification and the aperture along a path of one single crack varies quite significantly.

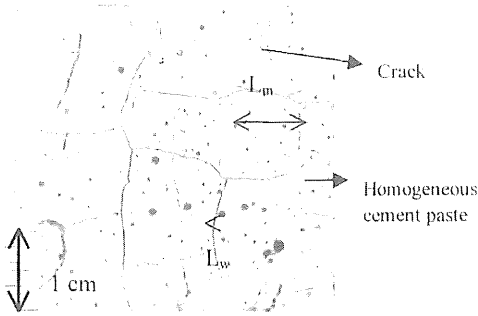


Figure 4: Crack network (impregnated with the red dye) superimposed to a homogeneous material for the specimen CO-2B.  $L_m$  is the mean crack spacing.  $L_w$  is the crack width.

The specimens such as 1B, 2A or 2B can be assimilated to a composite material in which the crack network is superimposed to a homogeneous material. The cracks induced by thermal treatment are not determined by MIP ( $L_w > 60 \mu\text{m}$ ). The porosity of the homogeneous material for each specimen is characterized by mercury intrusion porosimetry as shown previously and increases with the temperature of the thermal treatment.

### 3.2 Permeability

#### 3.2.1 Pre-conditioning

Figure 5 shows the evolution of the variation of the weight loss for specimen CO-1A, 2B and CN-1A, 2B during pre-conditioning ( $20^\circ\text{C}$ ,  $\text{RH}=90.4\%$ ).

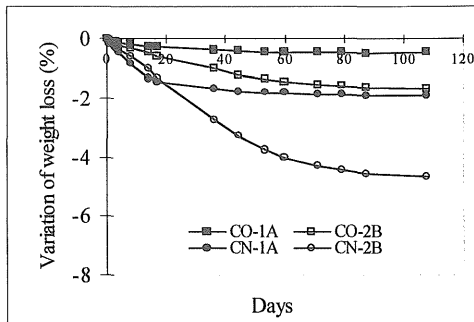


Figure 5: Variation of weight loss during pre-conditioning ( $T=20^\circ\text{C}$ ,  $\text{RH}=90.4\%$ ) for all specimens.

The curve represents the average value for the three specimens. Specimens 2B are drying faster than specimens 1A. Thanks to the choice of the pre-conditioning, only pores with widths of size  $10 \text{ nm}$  and larger are dried (according to the Kelvin-Laplace equation).

#### 3.2.2 Permeability test results

The gas permeability test results are given in Figure 9 and in Table 2. Three samples are tested per specimen and the measured permeability for each sample is represented in Figure 6.

Table 2. Results of gas permeability tests and of predicted values for the specimens 1A and 2B.  $K_{\text{exp}}$  ( $\text{m}^2$ ) is the average experimental value and  $K_{\text{the}}$  ( $\text{m}^2$ ) is the predicted result.

	CO		CN	
	$K_{\text{exp}}$	$K_{\text{the}}$	$K_{\text{exp}}$	$K_{\text{the}}$
1A	$1.9 \cdot 10^{-19}$ *	$1.8 \cdot 10^{-19}$	$1.2 \cdot 10^{-18}$	$6 \cdot 10^{-20}$
2B	$7.2 \cdot 10^{-19}$	$3.8 \cdot 10^{-18}$	$5.2 \cdot 10^{-18}$	$2 \cdot 10^{-18}$

\* Average on two values, except one value for CO-1A, which may be considered as non-significant.

Our results show that the experimental permeability  $K_{\text{exp}}$  can vary of an order of magnitude.  $K_{\text{exp}}$  is higher for the specimens CN than for the specimens CO. Furthermore  $K_{\text{exp}}$  is higher for the specimen 2B than for the specimen 1A. The difference between specimens 1A and 2B may be explained either by the modification of the porosity of the homogeneous material or by the presence of cracks.

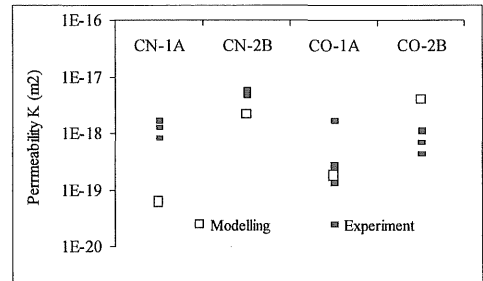


Figure 6: Experimental and predicted results for the gas permeability tests.

#### 3.2.3 Discussion

Katz-Thompson model is used in the following to analyze the effect of the microstructural parameters (porosity) on permeability  $K$  (Ollivier 1992). Based on percolation theory, the Katz-Thompson model establishes a relationship between permeability  $K$ , the formation factor  $F$  and the size of critical path  $d_c$  of a porous specimen:

$$K = \frac{d_c^2}{226F} \quad (3)$$

The diameter  $d_c$  is traditionally determined by using the mercury curve of the specimen (Table 1). The formation factor  $F$  is given as a function of the diameter  $d_c$  (Katz 1987) for very broad pore size distribution and for hydraulic conductance, such as:

$$F = \frac{d_{\max}}{d_c} \Phi S(d_{\max}) \quad (4)$$

where  $d_{\max} = 0.61.d_c$ ; and  $S$  = fractional volume of connected pore spaced involving pore widths of size  $d_{\max}$  and larger.

From Eq. 3 and Eq.4, the theoretical permeability  $K_{\text{the}}$  may be estimated. The predicted values  $K_{\text{the}}$  are given in Figure 6 and in Table 2 and are compared to the experimental values  $K_{\text{exp}}$ . This comparison is possible because only pores with widths of size 10 nm and larger contribute to permeability  $K_{\text{exp}}$ .

The theoretical values  $K_{\text{the}}$  are about the same as the experimental values  $K_{\text{exp}}$ . For the specimen CN-1A the predicted permeability  $K_{\text{the}}$  seems to be underestimated compared to the experimental value  $K_{\text{exp}}$ . This difference may be explained by the fact that the pore size distribution is not broad in this case compared to the one of the others specimens. Furthermore, the tendency given by the predicted values is quite similar to the tendency given by the experimental values. This comparison allows us to conclude that the permeability is influenced by the porosity of the homogeneous material.

Furthermore, the heterogeneities of microstructure due to cracking are not well characterized by the determination of the permeability coefficient because it is a macroscopic measure, which doesn't distinguish the different channels for the transport of gases. The contribution of the crack network on the volume flow rate of air  $Q$  is certainly weak compared to the one of the porosity of the homogeneous material. Then the measured permeability  $K_{\text{exp}}$  is certainly more influenced by porosity than by cracking. This result may be explained by the fact that the cracks are discontinuous (at high magnification) and that their width is less than 100  $\mu\text{m}$ . As mentioned by several authors and reported by Aldea et al. (1999) for water permeability tests performed on concrete, the increase of the permeability  $K$  is all the higher as the crack opening is high (above 100  $\mu\text{m}$ ). The experimental results (and the tendency) should be verified on the others specimens (1B and 2A) to confirm this conclusion.

### 3.3 Chloride diffusion process

#### 3.3.1 Experimental results

The chloride ingress is determined by colorimetric method as explained previously. The results of depth of chloride penetration are given in Figure 7 for the specimens CO-1A, 2B. The results for all specimens are given in Table 3.

In the case of the specimens CO-1A and CN-1A, the color change border is rather linear and is characterized in Figure 7a by a dotted line. In the case of the others specimens (CO, CN- 1B, 2A and 2B), the

separation between the two zones (zone A without chloride ions and zone B with chloride ions) is a little more irregular and is characterized in Figure 7b by a continuous line. Unfortunately, color pictures can not be reproduced in this document and the reader will not be able to distinguish well the color change border.

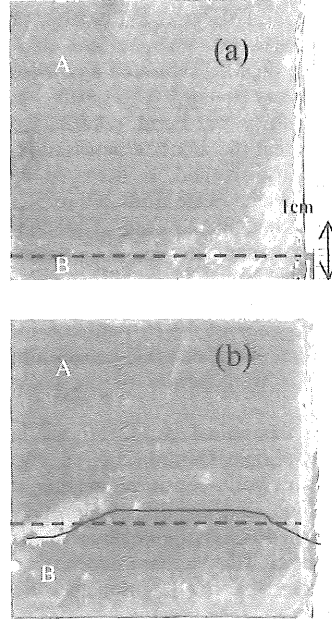


Figure 7: Chloride ingress revealed by colorimetric method for the specimens CO-1A (Figure 7a) and CO-2B (Figure 7b). Zone A: without chloride ions, Zone B: with chloride ions. Dotted line: average depth of chloride penetration, Continuous line: color change border.

Furthermore, an average depth of chloride penetration may be determined and is given in Table 3 for each specimen. The average depth, which may be considered as a macroscopic measure of the chloride penetration, is higher in the specimens (1B, 2A and 2B) than in the specimen (1A). This difference may be explained either by the modification of the porosity of the homogeneous material or by the presence of cracks.

Table 3. Results of chloride ingress for all specimens.  $X_{\text{cl}}$  is the depth of chloride penetration determined by colorimetric method.

	CO		CN	
	$X_{\text{cl}}$ (mm)		$X_{\text{cl}}$ (mm)	
1A	4		8	
1B	7.5		14	
2A	11		17	
2B	15		20	

### 3.3.2 Discussion

To verify the fact that cracking may influence the chloride penetration, a crack, induced by thermal treatment, is simulated by a notch with saw-cut. This artificial crack is straight and its width ( $L_w = 300 \mu\text{m}$ ) is larger than the one of the crack induced by thermal treatment ( $L_w < 100 \mu\text{m}$ ). The chloride penetration determined by colorimetric method (Figure 8) is modified by the presence of the artificial crack (the specimen has been completely immersed into chloride solution so that the crack is saturated and there is no coupling with capillary suction). This result is in accordance with previously published results. De Schutter (1999) shows that the chloride penetration, determined by colorimetric method, is increased by artificial straight cracks which range from 200 to 500  $\mu\text{m}$ . This result shows that, in the case of straight cracks, the colorimetric method allows us to distinguish the different channels for the transport of chloride. The superposition of the effect of several straight cracks, at a distance of 10-15 mm, can induce an increase of the depth of chloride penetration  $X_{Cl}$  and can explain the irregularities of the color change border.

Furthermore, from theoretical considerations in the case of steady-state regime, Gérard (2000) shows that an isotropic crack network, consisting in straight and connected cracks, increases the diffusive properties of chloride in cracked material compared to the one in uncracked material. This increase depends on the characteristics of the network (the mean aperture of the cracks and the mean crack spacing) and on the diffusive properties of the composite material (the diffusion coefficient  $D_1$  of chloride ions in the crack and the diffusion coefficient  $D_0$  in the uncracked material). According to Gérard (2000), the diffusion coefficient  $D$  of the cracked material in the case of an isotropic cracking pattern is given in Eq. 5:

$$\frac{D}{D_0} = \frac{2}{f} \cdot \frac{D_1}{D_0} + 1 \quad (5)$$

where  $f = L_w/L_m =$  crack spacing factor and for  $f \gg 1$ . For an isotropic cracking pattern such as described in Figure 4 ( $L_m \approx 12.5 \text{ mm}$  and  $L_w \approx 75 \mu\text{m}$ ), for  $D_1 \approx 10^{-9} \text{ m}^2/\text{s}$  (diffusion coefficient of chloride ions in an ideal solution) and for  $D_0 \approx 5.10^{-12} \text{ m}^2/\text{s}$  (determined by means of simple diffusion experiments for cement pastes such as CO and CN given in François (2001)), the diffusion coefficient  $D$  of the cracked material is about equal to  $3.5 D_0$ . So in our work, on the assumption that the diffusive properties of material may be linked to the depth of penetration of chloride (chloride binding are negligible), the increase of the average depth of chloride penetration  $X_{Cl}$  can be explained by the straight and connected cracks, which form an isotropic network.

The previous modeling considers that the diffusion coefficient of the homogeneous material of the

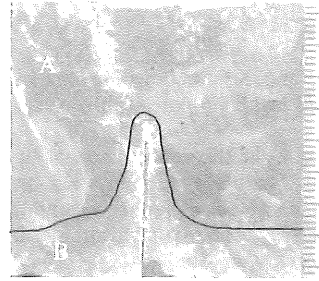


Figure 8: Chloride ingress revealed by colorimetric method for the specimen CN-1A with an artificial crack ( $L_w=300\mu\text{m}$ ).

cracked material is the same as the one of the uncracked material. This diffusion coefficient is related to the porosity of the material (Garboczi 1992). As the materials CN-1A and CO-1B have the same porosity (i.e. the same diffusive properties  $D_0$ ), the modeling given by Gérard (2000) for straight and connected cracks shows that the average depth  $X_{Cl}$  should be different for both materials. Nevertheless, experimental results are in contradiction with this conclusion. The average depth of chloride penetration for the uncracked material CN-1A is the same as the one for the cracked material CO-1B. These experimental results show that the used modeling is not valid and that cracking has no effect on the chloride penetration. As for gas permeability tests, this result may be explained by the intrinsic tortuosity of the cracks (the cracks are discontinuous at high magnification) and by their width (less than  $100 \mu\text{m}$  inferior to the width of the artificial crack - Figure 8- which is about  $300 \mu\text{m}$ ).

Furthermore, the crack network is quite similar for the specimens 1B, 2A and 2B, i.e. the crack spacing is the same and the average depth  $X_{Cl}$  of chloride penetration is different for these specimens. As the porosity  $\Phi$  of the homogeneous material of these materials is different, the depth of chloride penetration  $X_{Cl}$  has to be related to it. In order to analyze the effect of the porosity of the homogeneous material on the depth of chloride penetration, the relation between the depth of chloride penetration  $X_{Cl}$  and the total porosity  $\Phi$  is given in Figure 9.

Figure 9 shows that there is a very good correlation between the depth of chloride penetration  $X_{Cl}$  and the total porosity  $\Phi$ . This relationship shows that the chloride penetration is certainly more influenced by the porosity of the homogeneous material than by the cracking generated by thermal treatment. This result confirms that the chloride diffusion process in the cracks induced by thermal treatment has probably little influence on chloride ingress, although the front of chloride penetration is a little more irregular on specimens 1B, 2A and 2B than on specimens 1A.

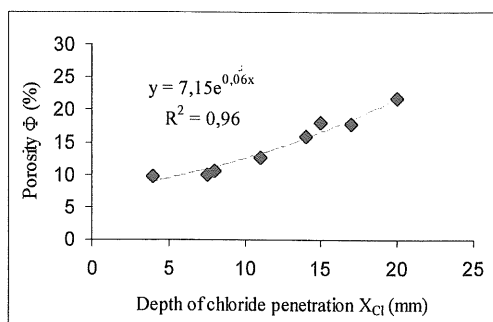


Figure 9: Relationship between the depth of chloride penetration  $X_{Cl}$  and the total porosity  $\Phi$ .

#### 4 CONCLUSIONS

The aim of this study was to determine the influence of localized microcracks induced by thermal treatment on transport properties. Materials (cement pastes) and experimental procedures are described. The thermal treatment induces an isotropic crack network, which is characterized by the mean aperture of cracks and by the mean crack spacing. Chloride diffusion and gas permeability tests are performed on uncracked and cracked materials.

Experimental results show that the heterogeneities of microstructure due to cracking are not well characterized by the determination of the permeability coefficient because it is a macroscopic measure, which doesn't distinguish the different channels for the transport of gases. The characterization of the chloride ingress by colorimetric method allows us to distinguish the different channels for the transport of chloride in the case of straight cracks. Nevertheless, the transport properties are not influenced by the cracks induced by thermal treatment. The influence of cracks is weak, certainly because of the width of cracks and their intrinsic tortuosity.

This work shows that the modification of the transport properties due to thermal treatment is explained by the modification of the porosity. So, in the case of chemical and physical actions which induce cracking, such as freezing-thawing or chemical attacks, the modification of porosity has to be investigated too.

In future works, influence of aggregates has to be considered to consider diffusive cracks localized in the paste-aggregate interfaces.

#### 5 REFERENCES

Aldea, C.M. & Shah S.P & Karr A. 1999. Permeability of cracked concrete. *Materials and Structures*, 32:370-376.  
 Caré, S. & Derxk, F. & Campin, J. 2000. Conception d'un perméamètre à charge variable. *Report of the Laboratoire central des Ponts et Chaussées*, in French.

Francois, R. & Francy, O. & Caré, S. & Baroghel Bouny, V. & Lovera, P. & Richet, C. 2001. Mesure du coefficient de diffusion des ions chlorures : comparaison régime permanent- régime transitoire. *Revue de Génie Civil*, in press.  
 Garboczi, E.J. & Bentz D.P. 1992. Computer simulation of the diffusivity of cement-based materials. *Journal of materials science*, 27: 2083-2092.  
 Gerard, B. & Marchand, J. 2000. Influence of cracking on the diffusion properties of cement-based materials. Part I: Influence of continuous cracks on the steady-state regime. *Cement and Concrete Research*, 30: 37-43.  
 Henry, D. Baroghel Bouny, V. & Chaussadent, T. 2000. Evaluation of chloride penetration into concrete by various methods. *2<sup>nd</sup> International RILEM Workshop on Testing and Modelling the chloride Ingress into Concrete*. 11-12 September 2000, Paris, France.  
 Hornain, H. Marchand, J. Ammouche, A. Commène, J.P. & Moranville, M. 1996. Microscopic observation of cracks in concrete - A new sample preparation technique using dye impregnation. *Cement and Concrete Research*, 26(4): 573-583.  
 Katz, A.J. & Thompson, A.H. 1987. Prediction of Rock Electrical Conductivity From Mercury Injection Measurements. *Journal of Geophysical Research*, 92(B1): 599-607.  
 Ollivier, J.P. & Massat, M. 1992. Permeability and microstructure of concrete: a review of modelling. *Cement and Concrete Research* 22: 503-514.  
 De Schutter, G. 1999. Quantification of the influence of cracks in concrete structures on carbonation and chloride penetration. *Magazine of Concrete Research*, 51(6): 427-435.  
 Yssorche, M.P. Bigas, J.P. & Ollivier, J.P. 1995. Mesure de la perméabilité à l'air dans les bétons au moyen d'un perméamètre à charge variable". *Materials and Structures*, Vol 28, pp. 401-405, 1995.